In-plane transport of photoexcited carriers in GaAs quantum wells

H. W. Yoon, D. R. Wake, and J. P. Wolfe
Materials Research Laboratory, University of Illinois at Urbana-Champaign, Urbana, Illinois 61801

H. Morkoç
Coordinated Science Laboratory, University of Illinois at Urbana-Champaign, Urbana, Illinois 61801
(Received 13 January 1992)

We have measured the picosecond-time-resolved in-plane motion of carriers in a multiple quantum well by a spatially scanned pump-probe technique at bath temperatures between 8.5 and 60 K. The effective ambipolar diffusivity measured from the spatial expansion of a nonequilibrium carrier distribution is found to increase with pump power, i.e., carrier density. We believe that this effect is in part due to the formation of a degenerate semiconductor plasma and to screening of scattering centers. An increase in the diffusivity is observed with the change in the bath temperature from 8.5 to 60 K that is consistent with a simple impurity-limited scattering model. The diffusivity at 0–200 ps is found to increase with the incident photon energy, while the diffusivity measured at 500 ps remains relatively constant with increasing photon energy. The decrease in the expansion rate with time is ascribed to the decreasing kinetic energies of the carriers.

I. INTRODUCTION

The properties of photoexcited carriers in $GaAs/Al_xGa_{1-x}As$ heterostructures have been extensively studied by spectroscopic means. Recently spatial techniques have been developed in order to understand the underlying mechanisms governing the transport of carriers. Time-of-flight measurements have been used to measure exciton transport, showing the dependence of diffusivity on the well width and the sample temperature.[1] An earlier study of exciton transport used an optical four-wave-mixing technique to measure transport and spatial localization effects,[2] and four-wave-mixing was also used to study ambipolar transport.[3] More recently a space- and time-resolved Raman probe has also been employed to examine the transport of plasma.[4] In our laboratory, the in-plane transport properties of photoexcited carriers have been measured using a scanned pump-probe technique which showed that the transport was dependent on initial pump intensity.[5,6]

This work presents a study of ambipolar transport in quantum wells and examines both the spatial expansion and spectral changes. Since the hot photoexcited carriers relax in energy while diffusing in space, the spectral and spatial evolution of nonequilibrium carriers optically injected in a localized region are interrelated. Despite this, no comprehensive time-resolved study of both of these phenomena under the same conditions has been reported. It is obvious that the local carrier density arising from an absorbed laser pulse depends on the excitation parameters, the carrier diffusivity, and the carrier lifetime. In order to develop a picture of both the spatial and the spectral properties, we have used a picosecond time-resolved spatial-imaging technique as in Ref. 5. Time-resolved information about photoexcited carriers is obtained by measuring their perturbation on the optical absorption spectra of the sample. The carriers excited by a pump pulse cause an increase in the transmission of a subsequent probe pulse. Absorption spectra are measured by overlapping the spatial position of the pump and probe beams. Both the pump and the probe beams can be sharply and independently focused as they pass through a multiple quantum well (MQW), and spatial information is gained by scanning either the pump or the probe beam parallel to the plane of the well, as shown in Fig. 1(a).[5] In an accompanying paper (hereafter referred to as paper I) we examine the influence of the nonequilibrium carrier density on the picosecond time-resolved transmission spectra at low temperatures. In this paper we concentrate on the time-resolved spatial expansion of photoexcited carriers in the MQW under the same conditions.

This paper is organized as follows: We describe the experimental procedure developed to obtain our spatial-spectral information. The lateral spread of carriers in the quantum well is quantitatively described by following the evolution of the full width at half maximum (FWHM or Δ) of the spatial carrier distribution. Experimental dependences of $\Delta(t)$ on bath temperature, T ($\approx$ lattice temperature T_L), and the photon energy of the pump pulse are described in terms of an effective diffusivity. We find that the observed dependence of the diffusivity on temperature and carrier density can be interpreted in terms of a model based on ionized impurity scattering.

II. EXPERIMENTAL METHODS

The schematic illustration in Fig. 1(b) depicts our experimental setup. The optical pulses are produced by Styrl-8 and Styrl-9 dye lasers synchronously pumped by a mode-locked argon-ion laser at 76 MHz. The wavelengths of the pump and probe lasers span an energy range near and above the band-gap energy. The spectral width of the laser pulses is approximately 0.4 meV, and

the cross-correlation width is <5 ps and stable to <1 ps. The time delay between the pulses is varied by a computer-controlled external delay line in the probe-beam path. The polarization of the pump beam is rotated 90° to the probe-beam polarization; the two beams are then made colinear at the polarizing beam splitter. The combined beam is focused onto the sample by a 10-mm focal-length achromat, L_3, which is fixed relative to the sample inside a variable-temperature optical cryostat operating in either a helium-immersion or a gas-flow mode. The light transmitted through the sample is focused onto a photodiode, and any residual (transmitted) pump light is blocked by a linear polarizer. Depending on the type of measurement, either the probe or the pump beam is mechanically chopped and the ac signal from the photodiode is fed to a lock-in amplifier.

For two-dimensional (2D) spatial imaging, the probe beam is raster scanned across a region containing the pump-beam spot [Fig. 1(a)]. To accomplish this, the probe beam is focused by lens L_2 at a spot before the Lucite refracting blocks, labeled x and y. The rotation of the Lucite blocks about orthogonal axes by electronically controlled galvanometers translates the focused spot on the sample. Lenses L_2 and L_1 independently determine the focus and position of the probe and pump spots on the sample. In order to calibrate the spatial scan range and to determine the spot size of the beams in the plane of the sample, metallic crosses with 10-μm-wide lines were deposited on the surface of the sapphire substrate. After adjusting the focal spots with the target, the convoluted beam spot of the focused pump and probe beams has a FWHM of about 4 μm, implying that each beam has a FWHM of about 3 μm. Galvanometer rotation, time delay, probe-beam wavelength, and data acquisition are coordinated by a computer and displayed on a video monitor.

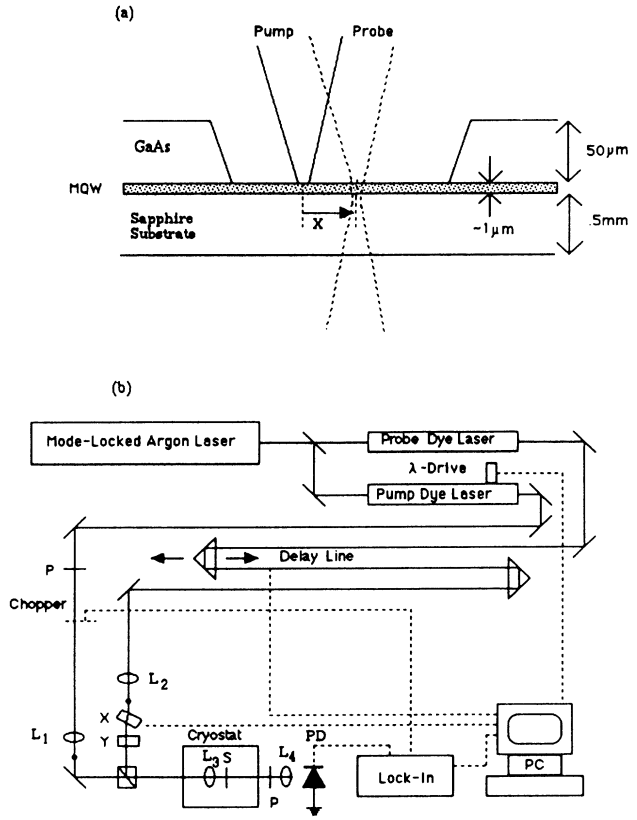

FIG. 1. (a) Diagram of MQW sample. The probe and the pump laser are focused into a 0.5-mm-diam region where the GaAs substrate has been etched away, leaving only the quantum-well structure mounted to the sapphire substrate. The pump and the probe beams can be independently translated. (b) Schematic of the picosecond absorption-imaging apparatus, as described in the text.

The sample used in this work is a MQW with 30 periods of 210-Å GaAs wells and 100-Å barriers of $Al_{0.25}Ga_{0.75}As$. The sample is glued with cyanoacrylate ("super glue") to a 0.5-mm-thick sapphire substrate with the c axis perpendicular to the wells. The GaAs substrate is etched away over a 0.5-mm-diameter region to provide a transmission window through the wells.[7] A spatial scan of the etched region shows inhomogeneities in the local spectrum. Since we are able to determine variation in the spectrum with a few-micron spatial resolution, etch pits and defects in the sample show up clearly in the image. In taking data, we avoided the regions with large inhomogeneities.

Time-resolved transmission spectra are recorded with the pump and probe beams positioned to pass through the same spot in the MQW window. Figure 2 shows transmission spectra taken by stepping the wavelength of the probe-laser pulse at fixed time delay with respect to

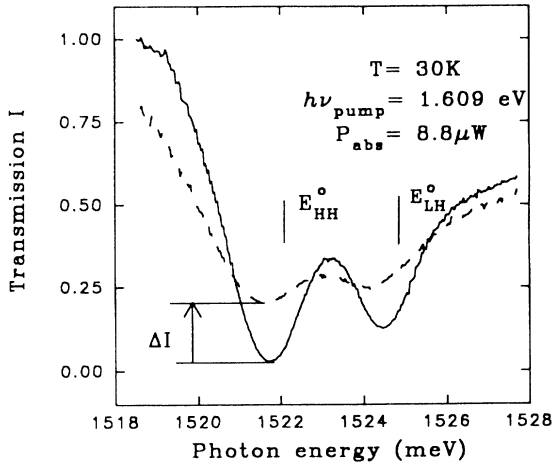

FIG. 2. Transmission spectrum of the probe beam at $x=0$ [Fig. 1(a)] and bath temperature of 30 K, measured by varying the probe wavelength. Heavy-hole (HH) and light-hole (LH) absorption lines are seen. The transmission I is normalized to the MQW transmission for a photon energy just below the gap (1.518 eV). The solid curve is the transmission measured by a nonperturbing probe beam with no pump pulse, and the dashed curve is the transmission measured 10 ps after the pump pulse. P_{abs} is the average pump power absorbed by the MQW. For zero pump power, the transmission of the probe beam at the HH resonance is 0.03, corresponding to an absorbance of 5×10^4 cm^{-1}.

the pump pulse. The intensity of the probe beam is reduced to roughly $\frac{1}{3}$ of the power level below which no self-induced perturbations are observed in the spectra (0.4 μW in a 4-μm-diam spot). The solid curve is the probe spectrum with the pump beam off, and the dashed curve shows the changes induced in the probe spectrum at a time 10 ps after the peak of the pump pulse. The heavy-hole and the light-hole exciton energies are in agreement with the well-width and barrier parameters described above.[8] A more detailed investigation of these spectra is the subject of the accompanying paper I.

To quantitatively study the carrier diffusion, we need to relate the observed changes in transmission to the number of carriers in the path of the probe beam. The total initial number of carriers is proportional to the absorbed energy per pulse at the pump wavelength, which in turn is related to the average incident power by the relation $E_{\text{pulse}}=P_{\text{abs}}/f=(\eta P_{\text{inc}}-P_t)/f$, where η is the fraction of the incident power that passes into the sample, P_t is the transmitted power, and $f=76$ MHz is the pulse repetition rate. ηP_{inc} is determined by measuring the maximum transmitted power, P_t^0, at a photon energy below the band gap (e.g., $h\nu=1.518$ eV in Fig. 2) where the absorption is assumed to be insignificant. The difference between this power and the power measured when the laser is tuned to $h\nu_{\text{pump}}$ above the band edge is the total power absorbed by the MQW, P_{abs}. For a typical $h\nu_{\text{pump}}=1.6$ eV, $P_{\text{abs}}/P_t^0=0.90$, implying that the power absorbed by a single well is on average $[1-(0.10)^{1/30}]P_t^0\approx 0.07P_t^0$, or roughly 7% of the power passing through the well. The 30 quantum wells serve to increase the optical absorption signal, but produce a variation in carrier density from front to back of a factor of 6–9 depending on photon energy. As a representative value, the average single-well carrier density at a pump power of $P_{\text{abs}}=1\mu$W is $n=1\times 10^9$ cm^{-2} for a FWHM spot diameter of 4 μm. All laser powers specified in the figures refer to P_{abs}. The carrier density estimated in this way represents the peak density obtained during the laser pulse.

Figure 3(a) shows the relationship between the pump-induced change in the transmission, ΔI, and the incident pump power for a fixed probe delay at 12 ps. ΔI is scaled to be between 0 for no bleaching and 1.00 for no probe absorption. A saturation in ΔI is clearly observed above 30 μW, and a linear relation between ΔI and P_{abs} is approached only below about 4 μW, corresponding to less than 10% change in transmission. The range of linearity may be extended by spatially integrating ΔI about the pump spot and plotting this versus P_{abs}. The result, plotted in Fig. 3(b), shows a nearly linear dependence up to about 50 μW. This analysis demonstrates that part of the "saturation" effect observed in Fig. 3(a) arises from the spread of carriers laterally from the initial excitation region. We also see from a comparison of Figs. 3(a) and 3(b) that one cannot assume a linear relationship between ΔI and the carrier density for ΔI in excess of about 50% bleaching. Within these qualifying limitations, however, the density can be approximated by the measured change in the transmission, $\Delta I(t)$.

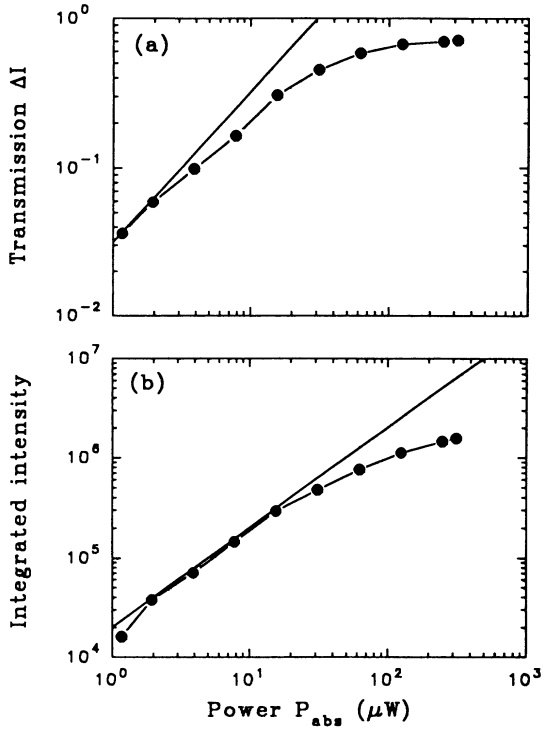

FIG. 3. (a) Carrier-induced transmission of the probe beam ΔI (defined in Fig. 2), as a function of the pump power. Both beams are spatially fixed and concentric (i.e., $x=0$ in Fig. 1), and the time delay between them is 20 ps. (b) Spatially integrated transmission intensity obtained by scanning the probe beam across the pump spot and assuming cylindrical symmetry. ($\Delta I\times\Delta^2$ in Fig. 5). This quantity exhibits a more-linear dependence on excitation power than the peak, ΔI, indicating that the saturation of ΔI in (a) is in part due to diffusion of carriers out of the pump region. The slopes of the lines are unity.

III. TIME-RESOLVED IMAGING OF 2D TRANSPORT

The capabilities we have described provide a sophisticated tool to study carrier motion with picosecond resolution. We effectively create a "movie" of the expansion process by measuring the x-y profile of the carrier distribution at a series of delay times. A time-resolved two-dimensional image produced by raster scanning the probe beam in the x and y directions is displayed in Fig. 4(a). The wavelength of the probe beam is fixed at the center of the heavy-hole exciton absorption line. The peak in the middle of Fig. 4(a) is due to the carrier-induced differential transmission, ΔI, of the probe beam 20 ps after the pump pulse. Figure 4(b) shows the enhanced transmission in the same region 1000 ps after the pump pulse. We see a reduced height and broadened width of the carrier distribution, indicating carrier recombination and lateral spatial expansion.

The rate of expansion of the carrier distribution over time is readily measured from information contained in these 2D images; however, the axial symmetry of the distribution indicates that the spatial distribution is com-

pletely characterized by a one-dimensional scan "through the peak." The line scans in Fig. 5(a) taken at a bath temperature of 40 K show the expansion in space of the carrier distribution as well as the decrease in height due to recombination. In this example, the time-averaged pump power absorbed by the crystal is $P_{abs}=195$ μW, corresponding to a pulse energy 2.6 pJ. To more clearly show the expansion as a function of time, the spatial profiles in Fig. 5(a) are scaled to the same maximum height and replotted in Fig. 5(b). The square of the FWHM as a function of time, $\Delta^2(t)$, is plotted for several pump powers in Fig. 6(a).

First we consider if $\Delta(t)$ adequately represents the spatial motion of the carriers. A bimolecular recombination term, proportional to $-Bn^2$, would tend to decrease the peak of the distribution more rapidly than the flanks, causing the shape of the distribution to flatten with time

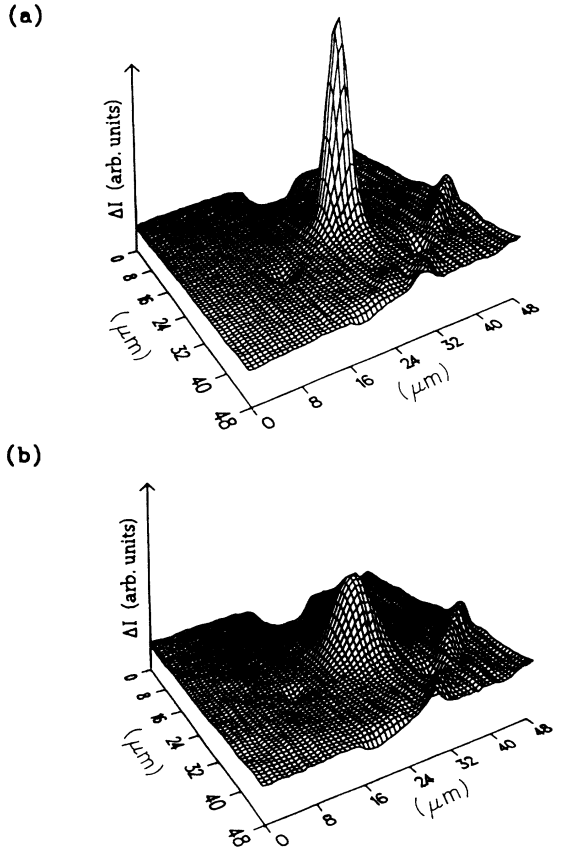

FIG. 4. (a) The transmitted probe intensity at the HH resonance as a function of position 20 ps after the pump pulse. The peak in the middle shows the enhanced transmission of the probe (i.e., "bleaching") due to the presence of carriers. The trough at the upper edge is due to blockage of a 10-μm-wide metal strip deposited on the surface of the sample for spatial calibration. The larger structures in the foreground are due to variations in the exciton spectrum due to local inhomogeneities. (b) The same spatial scan shown 1000 ps later. The bleached region has expanded due to carrier diffusion, and the integrated intensity is reduced as the carriers recombine. The two plots have the same absolute scales. The bath temperature is 40 K.

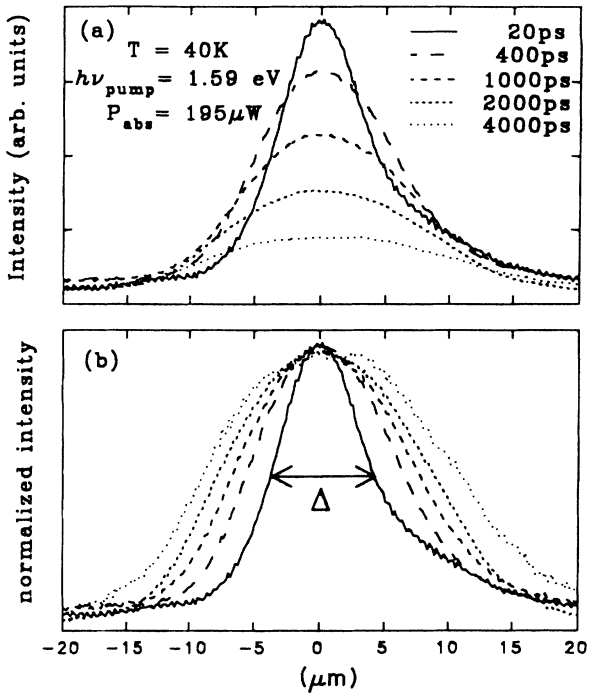

FIG. 5. (a) Line scans across the transmission peak for a series of delay times. (b) Same as in (a) but with the peak intensities scaled to the same value. The Δ denotes the full width at half maximum. These data clearly show the spatial expansion of the photoexcited carriers.

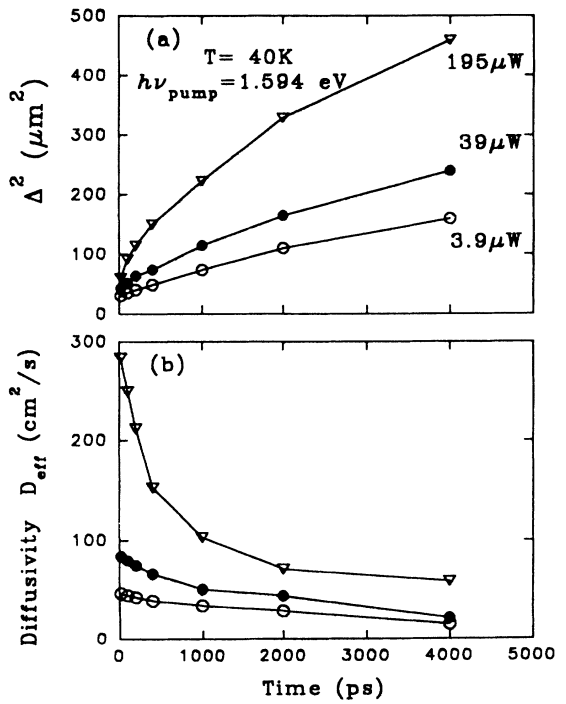

FIG. 6. (a) The square of Δ as a function of time for different pump powers, showing an increase in effective diffusivity with power. The curves are drawn to guide the eye. (b) The effective diffusivity is measured from the slope of Δ^2 vs time.

and lead to an apparent rapid motion of the carriers as measured by the FWHM. To test this possibility, line scans of a defocused 35-μm-wide distribution were measured as a function of time, then scaled to the same maximum height for comparison, as in Fig. 5(b). No change was observed in the width or shape of the distribution with time, indicating that bimolecular recombination terms were not significant. The carrier densities obtained in the wide defocused spot were lower than the highest densities studied in our experiments, so the relevance of the test is limited to medium to low carrier densities. More qualitatively, line scans taken at high density did not greatly depart from the general Gaussian shape observed at lower densities, indicating an insensitivity to density-dependent terms. Accordingly, we approximately characterize the expansion of the carrier distribution by measuring the time dependence of the FWHM alone.

For a purely diffusive process, one expects the expansion to be described by the two-dimensional diffusion equation,

$$\frac{\partial n}{\partial t}=D\frac{1}{r}\frac{\partial}{\partial r}\left[r\frac{\partial n}{\partial r}\right]-\frac{n}{\tau} \tag{1}$$

where the expansion is cylindrically symmetric and τ is the recombination time. For an initial Gaussian-shaped distribution, the solutions are of the form

$$n(r,t)=\frac{\sigma_0^2 n_0}{4Dt+\sigma_0^2}\exp\left[\frac{-t}{\tau}\right]\exp\left[\frac{-r^2}{4Dt+\sigma_0^2}\right] \tag{2}$$

where σ_0 is the initial $1/e$ half-width. The diffusivity, D, is obtained from the slope of the curve of Δ^2 versus time using the relation[9]

$$\Delta^2(t)=\Delta_0^2+11.09Dt \tag{3}$$

where $11.09=16\ln(2)$ and $\Delta_0^2=4\ln(2)\sigma_0^2$ is the initial (FWHM)^2 determined by the laser spot size on the sample.

We see from Fig. 6(a) that Δ^2 does not increase at a constant expansion rate as predicted by Eq. (3), but instead increases at a rate that monotonically decreases. Also, the expansion rate increases strongly with increasing carrier density, a parameter which does not enter the simple diffusion description. We define an effective diffusion constant, $D_{\rm eff}$, as the instantaneous value of $d\Delta^2/dt$ divided by 11.09, which may be approximated as the slope between adjacent data points, or the slope of a smooth curve fit to the data. Figure 6(b) shows how $D_{\rm eff}$ decreases with time for the three different initial excitation densities. For a given initial density, the effective diffusivity is seen to decrease in time by over a factor of 4.

The remainder of the paper examines the experimental factors responsible for the time- and density-dependent diffusivity noted above. We emphasize the roles of the carrier density, carrier velocity, plasma versus excitonic state of the carriers, and impurity scattering. Although this analysis provides insights into the carrier expansion process, we find that no simple model emerges that is capable of completely describing the behavior that we observe.

We first attempt to separate the effects of carrier temperature and density on the diffusivity by resonantly exciting at the heavy-hole (HH) exciton in order to minimize the kinetic energy of the carriers. As discussed in paper I, nonresonant photoexcitation initiates the carriers in a hot distribution with the carrier temperature $T_c > T_L$ for the carrier densities and time resolution in our experiments. The carriers cool through phonon emission with a time constant $\sim$250 ps that appears to increase slightly with increasing density.[10] Figure 6 depicts the expansion of carriers which are losing excess energy with time while decreasing in density through recombination and expansion. Figure 7(a) shows the corresponding resonant excitation case at a sample temperature of 8.5 K. The time behavior of Δ^2 appears to divide into two regimes: at times before 100 ps, the slope of Δ^2 versus time is strongly dependent on the initial carrier density, whereas at times after 200 ps, the slope remains relatively insensitive to the changes in the initial density. From Fig. 6, we note that the faster expansion persists longer at 40 K (nonresonant excitation) than at 8.5 K (resonant), but that here too, the initial carrier density (pump power) primarily affects the expansion rate at early times.

One might immediately speculate about the origin of this time- and power-dependent diffusivity. Previous work at $T \leq 15$ K interpreted a similar effect in terms of a ballistic-phonon wind,[5] and such a mechanism may play

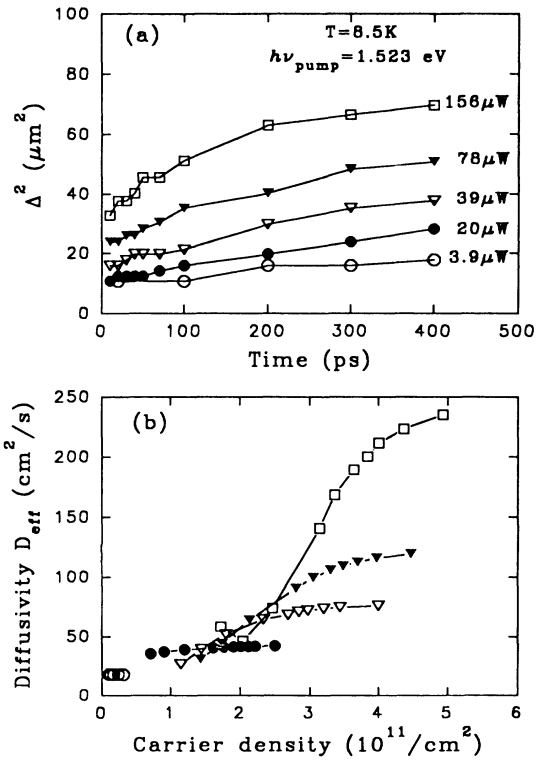

FIG. 7. (a) The square of Δ plotted as a function of time for the pump energy resonant with the HH exciton for various pump powers. (b) The effective diffusivity derived from the slopes of the curves in (a) as a function of carrier density.

some role in this data at 8.5 K. However, we find a similar density dependence in the expansion to occur when the lattice temperature is 40 K (Fig. 6) and the typical phonon mean free path is less than a few microns, arguing against a ballistic phonon-wind mechanism at these higher temperatures. Furthermore, in Fig. 6(a) the initial expansion velocity of the carriers at 195 μW is approximately 8×10^5 cm/s. This rate is greater than the velocity of sound ($v_s=5\times10^5$ cm/s for LA phonons in GaAs), which would not be expected from a phonon-wind-driven expansion.

In Fig. 7(b), the effective diffusivities are obtained from the slopes of smooth curves fit to the data in Fig. 7(a). Each curve of Fig. 7(b) portrays the expansion process, with time as a parametric variable increasing along the curves from right to left. The expansion rates of carrier populations may be compared for a particular density reached from different initial conditions. Notice that at high excitation levels the initial carrier density is not proportional to the excitation power because the initial Δ also increases with power, possibly due to a differential bleaching at high density [see Fig. 3(a) and the corresponding discussion]. The data of Fig. 7 demonstrate that there is not a simple one-to-one relationship between the carrier density and the diffusivity.

It is surprising that the diffusivity lacks a simple one-to-one relationship with carrier density. One possibility is that those carriers which start at a higher density have a greater kinetic energy. In other words, the distributions at $n=4\times10^{11}$ cm^{-2} in Fig. 7(b) have different effective temperatures. Retarded cooling rates have been previously observed at high carrier density in quantum wells, however, the present experiment involves near-resonant absorption. Another possibility is that the carriers increase in temperature due to Auger heating. The Auger mechanism seems to be especially relevant for resonantly pumped distributions in which the carriers are not excited with large excess energies. Unfortunately, a typical Auger coefficient for GaAs is on the order of 10^{-29}–10^{-30} cm^6/s,[11] whereas the magnitude necessary to appreciably affect the population within the first few picoseconds is 4×10^{-28}–1×10^{-26} cm^6/s. On the other hand, the Auger recombination may be enhanced by any mechanism that relaxes the constraint of momentum conservation in the scattering process.[12] If Auger recombination began during the laser pulse that resonantly excites the carriers, the heated carriers and nonequilibrium phonons generated would tend to promote the Auger nonradiative recombination coefficient until they cooled. Moreover, there is uncertainty in the size of the Auger coefficient in quantum wells, in large part due to uncertainty in the electron-hole overlap integral.[13] Only more precise calculations and experiments can reconcile the importance of Auger heating under intense photoexcitation in quantum wells, but presently we do not have another likely candidate to explain the boosted expansion rate at early times and high density [e.g., Fig. 7(b) for $n>3\times10^{11}$ cm^{-2}].

The diffusivity depends more on the instantaneous density than the initial conditions for $n<3\times10^{11}$ cm^{-2}. The diffusivity is observed to increase with increasing density in the range $(1-3)\times10^{11}$ cm^{-2} in Fig. 7(b), implying the existence of an electron-hole plasma for $n>1\times10^{11}$ cm^{-2}. A density-dependent scattering rate can arise first, from the increase in the kinetic energy of a degenerate plasma, and second, from the screening of ionized scatterers by the plasma. The density dependence of the exciton linewidth, discussed in paper I, suggests the dominance of the excitonic state at densities below $\sim1\times10^{11}$ cm^{-2}, whereas the density-dependent diffusivity above $\sim1\times10^{11}$ cm^{-2} suggests that a transition to the plasma phase at this density. In fact, these densities may be above the critical density, n_M, at which the metal-insulator transition is believed to occur. Some many-body calculations indicate a pseudo-2D Mott criterion of $n_M^{1/2}a\sim0.06$–0.08,[14] which yields $n_M=3\times10^9$ cm^{-2} for $a=138$ Å. Subsequent calculations suggest that $n_M^{1/2}a\sim0.8$ in 2D,[15] yielding $n_M=3\times10^{11}$ cm^{-2} for $a=138$ Å. Transmission experiments on an 180-Å well structure[16] and on modulation doped wells of 200-Å width also suggest a critical density at $\sim1\times10^{11}$ cm^{-2}.[17]

As pointed out by Hillmer *et al.*,[1] the plasma scattering rate will in general be different from that of the excitons. They suggested that the inverse scattering rate, or momentum relaxation time, is longer for plasma than for excitons, in apparent agreement with our results. Additionally, at low temperatures and at the higher densities in our experiment, the electronic-distribution function is expected initially to be degenerate with a quasi-Fermi energy in excess of $k_BT_{\rm bath}$. Thus screening of scattering centers and a higher average velocity of carriers in a degenerate distribution can explain the large initial ($t<100$ ps) diffusivity which increases with the carrier density.

The dependence of $D_{\rm eff}$ on carrier velocity may be examined independently of the density dependence by exciting near the band edge at a moderate initial carrier density $\leq10^{11}$ cm^{-2} over a range of bath temperatures. We assume that the carrier temperature remains near the bath (lattice) temperature during the expansion. Figure 8(a) shows expansion data for constant excitation density and $T=20$, 40, and 61.8 K. Under these conditions, the expanding carrier population should be nondegenerate and the LO-phonon population produced by carrier thermalization will be insignificant. Figure 8(b) shows the $D_{\rm eff}$ obtained from the slopes of the expansion curves for the three temperatures as a function of time and Fig. 9(a) replots these data points as a function of temperature. For simplicity, we assume an energy-independent scattering rate and mobility, consistent with measurement on n-type modulation-doped quantum wells with mobilities $\sim10^4$ cm^{-2}/V s. An energy-independent scattering time for a screened Coulomb potential over a 10–60 K temperature range agrees with calculations in the Born approximation to better than 10%.[18] The Einstein relation, or simply modeling the diffusivity as $\sim v^2\tau$ leads us to then expect that the diffusivity is linear in $T_c\sim\langle(mv^2)/2\rangle$ and Fig. 9(a) shows this to be borne out.[19] Figure 8(b) suggests, however, that the scattering time τ, must be decreasing with time as the density decreases with expansion and recombination. Thus we find that the "diffusion" of the two-component semiconductor plasma depends on both the average carrier velocity and

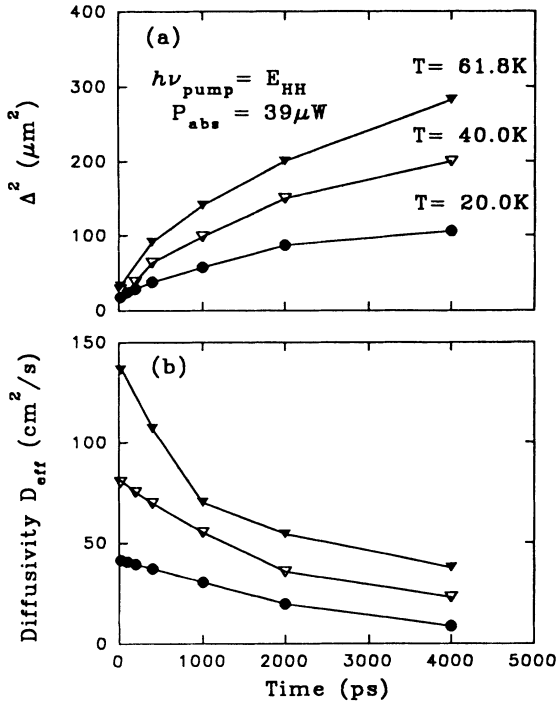

FIG. 8. (a) The square of Δ plotted as a function of time at different temperatures for the pump energy resonant with the HH exciton. (b) The effective diffusivity corresponding to the curves in (a).

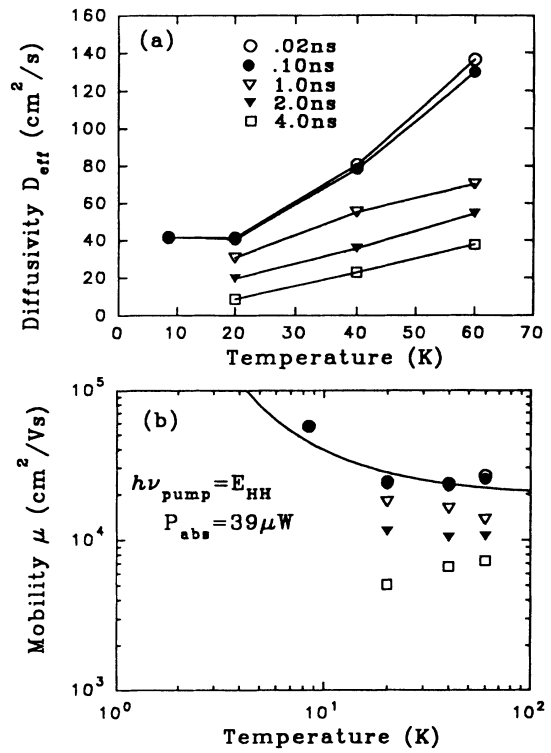

FIG. 9. (a) The diffusivity from Fig. 8(b) plotted as a function of temperature. (b) The mobility with the pump energy resonant with the HH exciton derived from (a) using the Einstein relation $D_{eff}=\mu k_B T/e$. The solid curve is calculated using a model for impurity scattering in two-dimensional structures, as described in the text.

the density-dependent scattering rate.

The value of the diffusivity and its temperature dependence at 700 ps is in agreement with luminescence measurements made under similar conditions by Hillmer *et al.*[1] Their time-of-flight luminescence experiments show a similar increase in diffusivity with temperature from 10 to ~70 K. The linear T dependence of the diffusivity was observed for a range of quantum-well widths from 80 to 740 Å. Our diffusivity data, determined from the spatial evolution of the differential absorption spectra, show a similar increase with temperature at a given delay time of 1 ns. Our data extend these results to show a more complex temperature dependence at earlier times which also depends on the delay time from the pump pulse.

We now return to the dependence of the expansion rate on the initial kinetic energy of the carriers. Studies have shown that electrons photoexcited by photon energies greater than the band-gap energy can achieve temperatures, T_c, much greater than the lattice temperature.[10] The carrier temperature determined from time-resolved luminescence data indicate that T_c can be as high as 150 K, with the lattice temperature at liquid-helium temperatures. The rate of decrease of the carrier temperature depends on the carrier density; a larger carrier density leads to a slower rate of decline in T_c, and the characteristic time for the drop in T_c can be as long as 300 ps.

The dependence of D_{eff} on excess pump energy at early time is shown in Fig. 10 for $T=8.5$ K and 3.9-μW excitation-power level. The D_{eff} increases from 20 to 100 cm^2/s as the photon energy is increased by 30 meV. Further increasing the photon energy above 1.552 eV does

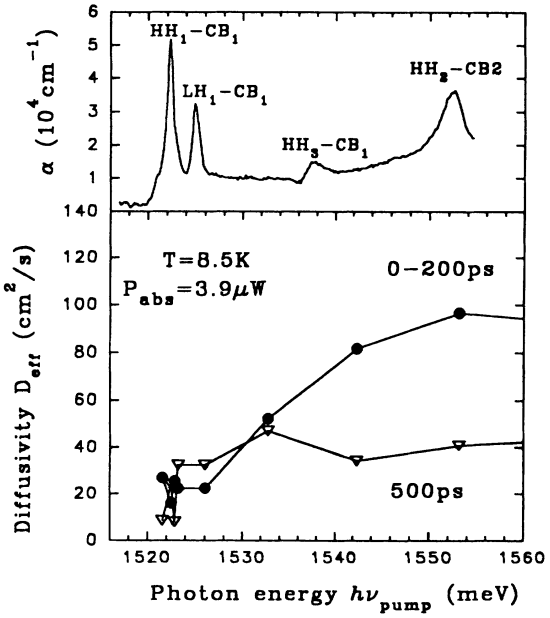

FIG. 10. (a) Absorption spectrum for the MQW as a function of probe-photon energy. The average diffusivity in two time regimes (0–200 ps and at 500 ps) plotted as a function of pump-photon energy. The higher diffusion rate at early times is likely due to the higher kinetic energy of particles at these times.

not lead to corresponding increases in D_{eff}, an observation we will shortly address. We believe that the increase in D_{eff} with excess energy is due to the more rapid carrier motion at the higher carrier temperatures. The cooling of the carrier distribution reduces the thermal velocity, so that at 500 ps the expansion rate is relatively independent of the initial excitation energy.

The saturation in D_{eff} as a function of the excess photon energy is probably caused by the rapid loss of energy of the carrier population due to the LO-phonon emission. The LO-phonon emission rate from a highly energetic electron is of order 150 fs and numerous studies have shown the importance of LO-phonon emission in limiting the effective electronic temperature.[20] This process acts to clamp the energy dependence of D_{eff} at an upper limit of approximately 30 meV for the times scales of interest in these experiments. Even if the carriers are created with a single kinetic energy somewhat less than that of an LO phonon, 36 meV, they scatter into a thermalized distribution with the same average energy, and a significant fraction can have kinetic energies larger than 36 meV. Hence, the cooling due to LO-phonon emission can be significant even when the average excess energy is well below 36 meV.

IV. DISCUSSION OF SCATTERING MECHANISMS

The excitation pulse creates a two-component semiconductor plasma in which the population density of the electrons is virtually equal to the density of holes, with both densities much greater than the density of impurities. The electron effective mass, $m_e^*=0.0665m_0$, is much lighter than the heavy-hole effective mass, $m_{\text{HH}}^*=0.45m_0$, where m_0 is the free-electron rest mass. The electrons move with a thermal velocity, $(m_e^*/m_{\text{HH}}^*)^{1/2}$ times the heavy-hole thermal velocity, or $v_e=2.6v_{\text{HH}}$. Thus, the electrons will attempt to move out from the photoexcitation spot more rapidly than the holes, but they lack sufficient thermal energy to significantly polarize the charge distribution. Therefore, the electron-hole population expands collectively as a neutral two-component plasma with an effective carrier mass limited mainly by the heavy holes. In the absence of external forces (e.g., phonon winds), the diffusivity measured in our experiment is thus an ambipolar diffusivity given by,[21]

$$D_{\text{eff}}=\frac{\mu_p D_n+\mu_n D_p}{\mu_p+\mu_n} \tag{4}$$

where μ_p (μ_n) is the hole (electron) mobility and D_p (D_n) is the hole (electron) diffusivity.

For a nondegenerate distribution, the Einstein relation connects the mobility and diffusivity: $\mu=eD/k_BT$. Even in degenerate distributions, D and μ are linearly related: $\mu=C(eD/k_BT)$ where C is a degeneracy-dependent constant[22] on the order of 1–10. In the nondegenerate case, the ambipolar diffusivity reduces to the expression $D_{\text{eff}}=2D_p/(1+D_p/D_n)$. The hole diffusivity is much less than the electron diffusivity because the hole mass and scattering cross section is greater than the corresponding electron quantities. Experimentally this is verified by the disparate mobilities measured in modulation-doped structures where $\mu_n/\mu_p\sim 10^6/(2\times 10^4)$. Thus $D_{\text{eff}}\approx 2D_p$, i.e., the expansion of the electron-hole system is determined by the hole diffusivity. The principle effect of the electrons may be to additionally enhance D_{eff} by screening the holes from scattering centers at high carrier density.

Various mechanisms can dominate the scattering rate depending on the particular conditions, including phonon scattering, interface roughness, and impurity scattering mechanisms. At the lattice temperatures employed here, the phonon populations for the resonant excitation case are small, and neither optical- nor acoustic-deformation-potential scattering is significant. For example, at 10 K acoustic-deformation-potential scattering for holes yields a mobility of $\sim 10^6$ cm^2/V s decreasing to $\sim 10^5$ cm^2/V s at 100 K, which would correspond to a T-independent diffusivity of 9×10^2 cm^2/s. Interface-roughness scattering is not expected to be important since the well width is relatively wide (210 Å), and well-width fluctuations cause very small perturbations in the electronic levels, possibly proportional to $1/L^6$.[23] The mechanism most likely to govern the expansion of the photoexcited population is therefore impurity scattering.

In modulation-doped GaAs quantum wells, the transport of the *one-component* electron plasma is governed by Coulombic scattering by background impurities for $T<80$ K. We have argued above that it is the hole mobilities which limit the transport of the *two-component* photoexcited plasma. The two-component plasma's hole scattering will be governed by a similar mechanism. Figure 9(b) shows the data of Fig. 9(a) transformed via the Einstein relation to the corresponding mobilities. Our experiments involve a complicated system in which the electrons and holes in the two-component plasma can have either degenerate or nondegenerate statistics. To our knowledge this situation has not been theoretically treated in the literature.

Nevertheless, it may be useful to compare our results to those of a single-component plasma in modulation-doped wells. The relatively weak T dependence seen in the plot of μ vs T is similar to that exhibited by modulation-doped structures analyzed in a number of theoretical and experimental studies.[24] The solid line in Fig. 9(b) is calculated using a model for mobility limited by ionized-impurity scattering in the heavily screened limit[25]

$$\mu\cong\frac{4\pi S_1^2 h^3(\varepsilon\varepsilon_0)^2|\mathbf{k}|}{e^3 m^{*2} N_i}\ , \tag{5}$$

where S_1 is the screening parameter in the strong scattering limit set equal to $2/a_B^*$, where a_B^* is the effective Bohr radius in GaAs, m^* is the heavy-hole effective mass, ε is the high-frequency dielectric constant, and N_i is the density of ionized impurities. At a degenerate density, the average electron wave vector $|\mathbf{k}|=(2\pi n_c)^{1/2}$, where n_c is the carrier concentration. For our experimental conditions, $n_c\sim 4\times 10^{11}$ cm^{-2} at $t=0$. As the temperature is lowered the density of ionized impurities within the well

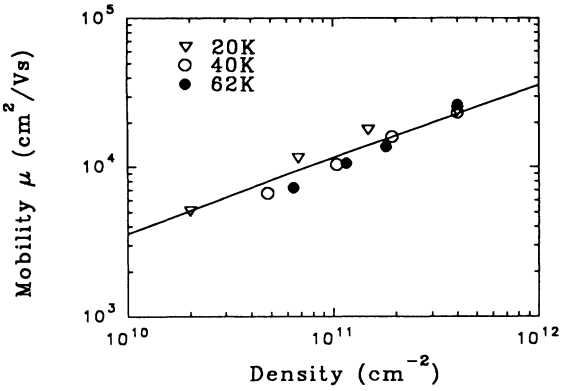

FIG. 11. The mobility from Fig. 9(b) plotted as a function of density. The density is obtained from the peak of the spatial distribution as a function of time. The line drawn shows $\mu \propto n^{\gamma}$, where $\gamma = 0.5$.

should decrease. In order to take into account the freeze out of the scattering centers, we have replaced the impurity density N_i by $N_0 \exp(-\phi/k_B T)$. The fitted curve in Fig. 9(b) was generated by using two adjustable parameters: the $N_0 = 3.3 \times 10^{14}$ cm^{-3} and the freeze-out energy $\phi = 0.6$ meV, which corresponds to 7 K. Furthermore, although not shown in Fig. 9, neutral-impurity scattering places an upper limit on the mobility as the sample temperature approaches $T = 0$ K.

In order to probe the idea that the dominant mechanism limiting carrier transport is the intrawell background impurities, the mobility seen at later times in Fig. 9(b) is plotted as a function of carrier density in Fig. 11. The mobility as a function of density follows an $n_c^{1/2}$ dependence, which agrees with the idealized model of Ref. 25 [their Eq. (27) with z_0 set $=0$]. The decrease in the mobility seen at later times in Fig. 9(b) follows from the reduction in the carrier density which corresponds to a decrease in the Fermi momentum: $k_F = (2\pi n_c)^{1/2}$. We note that most calculations of the density dependence of the mobility predict a $n_c^{3/2}$ dependence, whereas measured values span a range from $n_c^{1.0}$ to $n_c^{1.7}$ for $n_c > 1 \times 10^{11}$ cm^{-2}.[23] There exists one report that we are aware of that found a $n_c^{0.6}$ dependence,[26] for carrier densities ranging from 1×10^{10} to 1×10^{11} cm^{-2}. Thus we see that even within the one-component plasma, the situation remains uncertain, despite the excellent agreement between measured modulation-doped high-density mobilities and the theoretical values.

At high temperatures and at low densities, the model for scattering needs to take into account the changes in the carrier distribution from a degenerate distribution to a nondegenerate distribution. The degree of degeneracy can be determined by the comparison of the Fermi energy with $k_B T$. At a carrier density of 4×10^{11} cm^{-2}, the Fermi energy of electrons is 14.4 meV while the Fermi energy for the holes is 2.1 meV. At the highest temperature studied, the thermal energy is greater than the hole Fermi energy. Thus, initially the system of electrons and holes are in a degenerate state, but as the carriers decay by recombination, the electrons remain degenerate while the holes become nondegenerate. The mobility due to ionized-impurity scattering is predicted to decrease smoothly from the heavily screened degenerate limit exhibiting no temperature dependence to the nondegenerate lightly screened limit which shows a $T^{3/2}$ dependence.[27] The data in Fig. 9(b) does not show a strong temperature dependence, indicating that the low-screening limit has not been reached.

V. CONCLUSION

In summary, we observe an ambipolar diffusivity which is temperature dependent and consistent with the impurity-limited scattering model. The diffusivity decreases in time as the carrier density diminishes by recombination. The initial mobility at $t = 20$ ps, can be fitted with a two-dimensional ionized-impurity-scattering model in which the density of scatters is 3.3×10^{14} cm^{-3} and the freeze-out temperature is 7 K. The increase in diffusivity with the carrier density is likely due to the screening and the increased degeneracy of carriers, although we are in need of an appropriate detailed model with which to interpret our results. The average effective ambipolar diffusivity at early times (0–200 ps) increases with the pump photon energy, as the excess energy increases up to ~30 meV above the heavy-hole exciton energy. This increase in diffusivity is interpreted to originate from the higher carrier temperature generated by larger excess energies. The absence of an increase in D_{eff} with increasing pump photon energy above 30 meV is consistent with the emission of LO phonons which limit the rise in the carrier temperature. At 500 ps, no dependence of D_{eff} on excess energy is observed, indicating that by this time the carriers have cooled back to the bath temperature. While a number of previous studies have observed these cooling processes in semiconductors by time-resolved spectroscopy, our experiments may be the first to show how this cooling process manifests itself in the diffusivity of photoexcited carriers in a quantum well.

ACKNOWLEDGMENTS

This work is supported by DOE under MRL Grant No. DEAC02-76ER01198. The experiments were performed in the Laser Laboratory Facility of the Materials Research Laboratory.

[1] H. Hillmer, A. Forchel, S. Hansmann, M. Morohashi, E. Lopez, H. P. Meier, and K. Ploog, Phys. Rev. B **39**, 10 901 (1989).

[2] J. Hegarty and M. D. Sturge, Surf. Sci. **196**, 555 (1988).

[3] A. Miller, R. J. Manning, P. K. Milson, D. C. Hutchings, and D. W. Crust, J. Opt. Soc. Am. B **6**, 567 (1989).

[4] K. T. Tsen, O. F. Sankey, G. Halama, S. C. Tsen, and H. Morkoç, Phys. Rev. B **39**, 6276 (1989).

[5] L. M. Smith, J. S. Preston, J. P. Wolfe, D. R. Wake, J. Klem, T. Henderson, and H. Morkoç, Phys. Rev. B **39**, 1862 (1989).

[6]D. R. Wake, H. W. Yoon, J. S. Preston, H. Morkoç, and J. P. Wolfe, in *Ultrafast Phenomena VII,* edited by C. B. Harris, E. P. Ippen, G. A. Mourou, and A. Zewail (Springer-Verlag, Berlin, 1990), p. 262.

[7]R. A. Logan and F. K. Reinhart, J. Appl. Phys. **44**, 4172 (1973).

[8]W. T. Masselink, P. J. Pearah, J. Klem, C. K. Peng, H. Morkoç, G. D. Sanders, and Y. C. Chang, Phys. Rev. B **32**, 8027 (1985).

[9]D. P. Trauernicht and J. P. Wolfe, Phys. Rev. B **33**, 8506 (1986).

[10]K. Leo, W. W. Rühle, and K. Ploog, Phys. Rev. B **38**, 1947 (1988).

[11]B. K. Ridley, Phys. Rev. B **41**, 12 190 (1990).

[12]P. T. Landsberg, Solid State Electron. **30**, 1107 (1987).

[13]M. G. Burt, S. Brand, C. Smith, and R. A. Abram, J. Phys. C **17**, 6385 (1984).

[14]S. Scmitt-Rink and C. Ell, J. Lumin. **30**, 585 (1985).

[15]R. Zimmerman, Phys. Status Solidi B **146**, 371 (1988).

[16]C. Tränkle, E. Lach, M. Walther, and A. Forchel, Surf. Sci. **196**, 584 (1988).

[17]D. Huang, H. Y. Chu, Y. C. Chang, R. Houdré, and H. Morkoç, Phys. Rev. B **38**, 1246 (1988).

[18]F. Stern and W. E. Howard, Phys. Rev. **163**, 816 (1967); F. Stern, Phys. Rev. Lett. **44**, 1469 (1980).

[19]For a comparison to the T dependence of modulation-doped GaAs MQWS, see, e.g., P. J. van Hall, Superlatt. Microstruct. **6**, 213 (1989); K. Hirakawa and H. Sakaki, Phys. Rev. B **33**, 8291 (1986).

[20]E. M. Conwell, in *Solid State Physics,* edited by F. Seitz, D. Turnbull, and H. Ehrenreich (Academic, New York, 1967), Suppl. 9.

[21]W. Van Roosebeck, Phys. Rev. **91**, 282 (1953).

[22]A. H. Marshak and D. Assaf III, Solid State Electron. **16**, 675 (1973).

[23]H. Sakaki, T. Noda, K. Hirakawa, M. Tanaka, and T. Matusue, Appl. Phys. Lett. **51**, 1934 (1987).

[24]For a recent review, see J. J. Harris, J. A. Pals, and R. Woltjer, Rep. Prog. Phys. **52**, 1217 (1989).

[25]K. Hess, in *Advances in Electronics and Electron Physics,* edited by Peter Hawkes (Academic, New York, 1982), Vol. 59, p. 239.

[26]M. Shayegan, V. J. Goldman, C. Jiang, T. Sajoto, and M. Santos, Appl. Phys. Lett. **52**, 1086 (1988).

[27]K. Hess, *Advanced Theory of Semiconductor Devices* (Prentice-Hall, Englewood Cliffs, NJ, 1988).

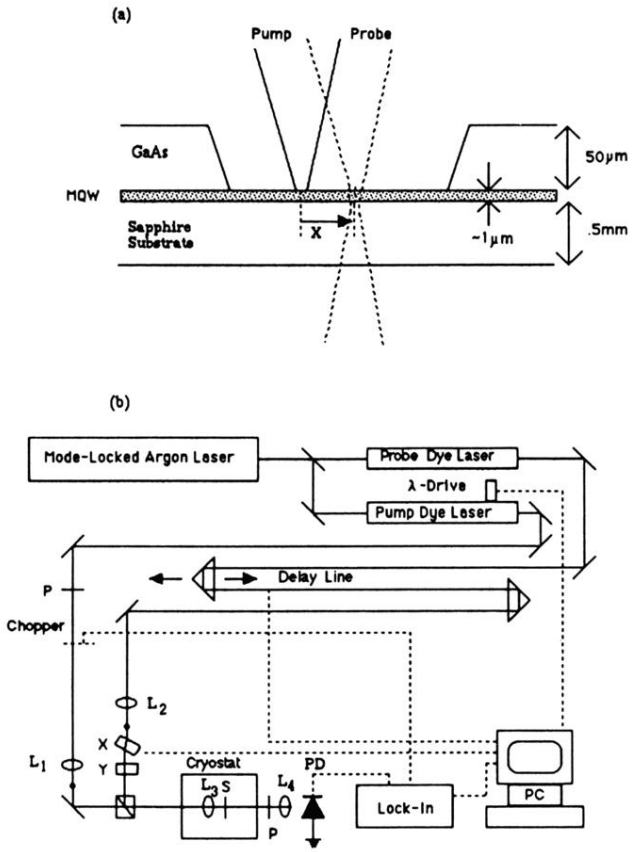

FIG. 1. (a) Diagram of MQW sample. The probe and the pump laser are focused into a 0.5-mm-diam region where the GaAs substrate has been etched away, leaving only the quantum-well structure mounted to the sapphire substrate. The pump and the probe beams can be independently translated. (b) Schematic of the picosecond absorption-imaging apparatus, as described in the text.

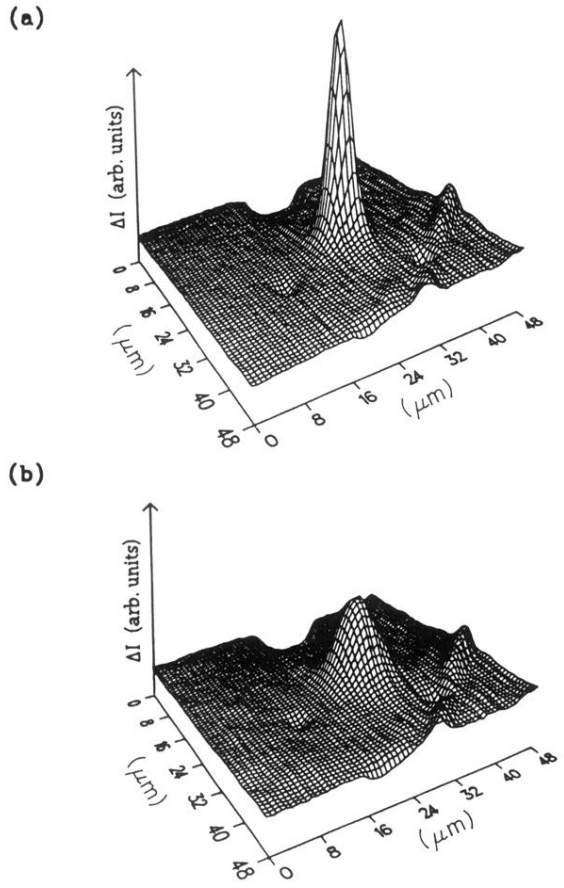

FIG. 4. (a) The transmitted probe intensity at the HH resonance as a function of position 20 ps after the pump pulse. The peak in the middle shows the enhanced transmission of the probe (i.e., "bleaching") due to the presence of carriers. The trough at the upper edge is due to blockage of a 10-μm-wide metal strip deposited on the surface of the sample for spatial calibration. The larger structures in the foreground are due to variations in the exciton spectrum due to local inhomogeneities. (b) The same spatial scan shown 1000 ps later. The bleached region has expanded due to carrier diffusion, and the integrated intensity is reduced as the carriers recombine. The two plots have the same absolute scales. The bath temperature is 40 K.